Experimed 2024; 14(1): 54-60

ORIGINAL ARTICLE

DOI: 10.26650/experimed.1425820

Assessing the Impact of Hypercapnic Stimulation on Brain Connectivity Metrics During Functional Magnetic Resonance Imaging

Idiz Iset [1], Ali Bayram[1]

[1]Department of Neuroscience, Aziz Sancar Institute of Experimental Medicine, Istanbul University, Istanbul, Turkiye

ORCID ID: I.I. 0000-0002-9764-7956; A.B. 0000-0002-6588-3479

Cite this article as: Iset I, Bayram A. Assessing the impact of hypercapnic stimulation on brain connectivity metrics during functional magnetic resonance imaging. Experimed 2024; 14(1): 54-60.

ABSTRACT

Objective: Functional connectivity serves as a widely employed metric in neuroscience research focusing on the dynamics of the brain. Additionally, non-neuronal physiological oscillations are acknowledged as being able to impact functional connectivity. This study aimed to explore the effects of non-neuronal hypercapnic stimulation on the activity of intrinsic connectivity networks (ICNs), as well as the dynamic changes in connectivity between them.

Materials and Methods: The study involved 10 healthy participants, encompassed their functional magnetic resonance imaging (fMRI) scans with carbon dioxide-enriched air stimuli in a block paradigm, with group independent component analysis (GICA) being used for defining ICNs. Similarity analysis has been conducted between the connectivity changes in the network components and the end-tidal partial pressure of carbon dioxide ($PETCO_2$).

Results: The study has identified 40 components representing 10 ICNs. Of these, 11 components representing seven ICNs were found to have significantly correlated time courses with $PETCO_2$. Among the networks without correlated components, the dynamic functional connectivity metrics of the language network and the subcortical network have been found to be significantly modulated by $PETCO_2$.

Conclusion: The cerebrovascular reactivity to a hypercapnic stimulus is a factor that influences changes in the blood oxygenation level-dependent fMRI signal. This non-neuronal effect is detectable for ICN components derived by the GICA technique and must be considered when making inferences about network connectivity metrics.

Keywords: Cerebrovascular reactivity, hypercapnic stimulation, functional magnetic resonance imaging, functional network connectivity, intrinsic connectivity networks

INTRODUCTION

Functional connectivity, commonly characterized as the coordination of activity among different brain regions, represents the communication and transfer of information within the brain. In order to investigate connectivity, one study conducted an examination of the similarity in blood oxygen level dependent (BOLD) signals from different brain regions through the use of functional magnetic resonance imaging (fMRI) during both task activations and resting state (1). Studies on resting state functional connectivity offer insights into the spontaneous low-frequency BOLD oscillations within the brain (2, 3). This approach is particularly preferred as it requires minimal active participation from subjects, thus allowing the detection of connectivity networks.

Intrinsic connectivity networks (ICNs, also known as resting state networks) refer to a collection of brain regions that exhibit similarities in their BOLD time series acquired during resting state. Investigating the dynamics of the brain using functional connectivity allows researchers to identify ICNs and evaluate cognitive tasks, conditions, and diseases from a network perspective. Functional connectivity analysis

Corresponding Author: Ali Bayram **E-mail:** ali.bayram@istanbul.edu.tr
Submitted: 26.01.2024 **Revision Requested:** 17.03.2024 **Last Revision Received:** 22.03.2024 **Accepted:** 14.04.2024 **Published Online:** 18.04.2024

of fMRI data and the detection of connectivity networks can be conducted through two fundamental methods. The first involves the detection of brain voxels correlated with the average BOLD response of a predetermined brain region or seed region based on a hypothesis (4). The second method employs a data-driven, exploratory approach known as independent component analysis (ICA) (5). ICA has the ability to extract meaningful information from complex data without the need for a priori anatomical assumptions or subjective selection of seed areas. Another aspect of ICA is its capability to isolate sources of noise to some extent. In functional neuroimaging, the presence of noise such as physiological artifacts or scanner-related distortions can significantly impact the quality and interpretability of the data. By decomposing mixed signals into independent components, ICA can help identify and separate out noise sources (6), thereby enhancing the signal-to-noise ratio and improving the overall robustness of the analysis.

While ICA can aid in isolating sources of noise, importance is had in recognizing that BOLD signal changes may indeed arise from non-neuronal sources. However, BOLD fMRI alterations may result from neuronal activation via neurovascular coupling, or they can originate from various other physiological processes influencing cerebral blood flow (CBF), oxygenation, or volume. In this sense, BOLD fMRI can be utilized not only for studying neuronal activity but also for assessing vascular health (7). This process is linked to cerebrovascular reactivity (CVR), which refers to the ability of blood vessels in the brain to dilate or constrict in response to a hypercapnic stimulus. Hypercapnic stimulation can be achieved by breathing carbon dioxide-enriched air or breath-holding, which in turn triggers an increase in CBF and results in an increase in the BOLD signal. Thus, CVR can be assessed by analyzing the variations of the BOLD signal during breathing paradigms (8). Importantly, given that both CVR and functional connectivity rely on the analysis of BOLD echo planar imaging (EPI), estimating connectivity parameters becomes plausible using CVR data.

This study aimed to explore how the BOLD response, which varies in response to a hypercapnic stimulus, impacts ICNs. This exploration is important for understanding the extent to which these networks, traditionally seen as neuronal, are influenced by physiological signals.

MATERIALS AND METHODS

MRI Dataset and Physiological Recordings

This study used the MRI data shared by Blockley et al. at the Oxford University Research Archive (9). The published research article that utilized this data focused on the feasibility of reliably calculating CVR maps within clinically acceptable scan durations. It explored the use of CO_2-enriched air with a sinusoidally modulated stimulus paradigm as an alternative to the Toronto block paradigm, in which the hypercapnic stimuli are administered in block form (9). Despite the sinusoidal breathing paradigm being considered a promising alternative, this study has chosen to use only the MRI data acquired during the Toronto breathing paradigm. Additionally, it utilized the partial pressure of end-tidal CO_2 ($PETCO_2$) data obtained during the MRI scans.

The MRI dataset comprises functional and structural images from 10 healthy participants (5 females; age range 19–21) and were acquired using a 3T scanner. The fMRI scans were consisted of 210 EPI volumes lasting 7 minutes, with time of repetition (TR) equal to 2000 ms and time of echo (TE) equal to 30 ms, covering the whole brain at a voxel size of 3.4 x 3.4 x 5 mm^3. Additionally, T1-weighted structural scans were obtained with 1.5 mm isotropic voxels. For the hypercapnic stimulation during functional imaging, a gas mixture (CO_2-enriched air) was breathed by the participants and administered using a gas blender (RespirAct™ Gen 3, Thornhill Research Inc., Toronto, Canada). The Toronto protocol had two hypercapnia blocks with an increase of 10 mmHg from the subject's specific baseline level of $PETCO_2$ and lasted 45 s and 120 s. The protocol has three baseline level periods: 1) lasting 60 seconds at the beginning, 2) lasting 90 seconds between two blocks, and 3) lasting 105 seconds at the end (10). Further details about the scanning parameters and experimental setup were described in the reference paper (9).

Data Analysis

Preprocessing

All preprocessing steps were performed using the program FMRIB's Software Library (FSL v6.0; www.fmrib.ox.ac.uk/fsl). Field maps and functional images were used during the preprocessing stages to cover motion and distortion correction and slice timing correction (11, 12). Structural and functional images were co-registered using a boundary-based registration method (13) and normalized to the Montreal Neurological Institute (MNI) space. Segmentation procedures were employed to derive grey matter masks for individual subjects. These masks were then utilized to compute the subject-specific global signal (GS) representing the average brain signal encompassed within this defined mask. Spatial smoothing with a 5 mm full width at half maximum (FWHM) kernel was applied as the final stage of preprocessing (14).

Group Independent Component Analysis

Preprocessed functional data were decomposed into functional networks using the Group ICA of fMRI Toolbox (GIFT; http://mialab.mrn.org/software/gift/), and 100 common spatially independent components (ICs) were detected (15). Variance normalization was applied prior to the GICA analysis. In the first stage of dimension reduction, 200 subject-specific principal components were obtained. Subsequently, a second-dimension reduction was implemented on the aggregated group data that was composed of sequentially added principal components from all participants, resulting in 100 principal components. The Infomax algorithm was utilized to maximize the spatial independence of the data (15). To increase the reliability of the ICA algorithm, the procedure was repeated 20

times with the ICASSO method, in which the most central run was chosen as the resulting IC. A group information-guided ICA (GIG-ICA) approach within the GIFT was used to derive subject-specific ICs that match the obtained group components while preserving their spatial independence (16).

The commonly used method in the component labeling process is the visual inspection of three complementary pieces of information from the components: the spatial map, time series, and spectral power (17). As a result of the evaluation, 40 of the 100 components were defined as the network components of the ICNs. The cortical network atlas of the program Functional Connectivity Toolbox (CONN v20b) (18) and the network parcellation atlas of Yeo et al. (19) were used to label the network components. Additionally, the subcortical network was labeled, as it had not been defined in either atlas.

The Similarity of Time Courses Between the Network Components and $PETCO_2$

To investigate the level of temporal similarity, the study employs a comprehensive analysis pipeline as illustrated in Figure 1. The focus centers on assessing the correlation between the time course of the $PETCO_2$ and the defined network components. To ensure accurate temporal alignment before the correlation analysis, the study employs GS as the reference signal. Calculating the GS involves transforming the gray matter probabilistic map produced in the segmentation stage into a mask consisting of voxels above a threshold value of 0.5 and then extracting the average BOLD time series of the gray matter mask.

The reference GS was initially utilized to correct the temporal delay of the $PETCO_2$ time course for each subject by employing cross-correlation, thereby ensuring synchronization (time-locked) with the GS. The open-source Rapidtide v2.2.7 software package (20) was used for the cross-correlation calculation. Further refinement was performed by adjusting the temporal position of the $PETCO_2$ time course using component delay times relative to the GS. However, the conventional cross-correlation method, which identifies time delays based on maximum correlation, was deemed unsuitable due to potential uncorrelatedness between the ICA-derived component time courses and the $PETCO_2$ time course. Consequently, component delay times were determined using the average time courses within the component maps. A threshold ($t > 2.0$) was applied to the spatial map of the relevant component, and the gray matter mask was multiplied while creating the component ROIs. The average signal within the component ROI was calculated, and the time delay of this signal as detected through cross-correlation with GS was considered to be equal to the time delay of the corresponding component time course. Delay times for the 40 components were used separately to correct the time lag between the component time courses and $PETCO_2$ time course, and then the correlation coefficients were calculated (Figure 1).

Statistical Analyses for Time Series Correlation

Random $PETCO_2$ signals were selected from each participant's own post-calibration period for use in the non-parametric statistical analysis in order to make a noise estimate. This process was repeated for each participant, with the $PETCO_2$ signal taken from 10 random time periods obtained by shifting 10 s. A total of 100 random correlation values (10 for each participant) were found in the resulting random correlation pool. Fisher's z-transformation was applied to the correlation values before making the statistical inference. Statistical analysis was performed using SPSS (IBM SPSS Statistics, v22; https://www.ibm.com/tr-tr/products/spss-statistics) to test whether the coupled correlation value differed from this random correlation pool with an independent samples t-test, with a multiple-comparison correction (Bonferroni correction) being applied to the results.

$PETCO_2$-Modulated Dynamic Functional Network Connectivity Analysis

The study assesses the $PETCO_2$ signal's modulation of the dynamic functional connectivity change between ICN component pairs. This involves computing sliding-window correlation coefficients between the time-courses of ICN components, referred to as dynamic functional network connectivities (dFNCs) and subsequently assessing $PETCO_2$'s modulatory effect on the resulting dFNCs through regression analysis. The GIFT toolbox (21) was utilized for the sliding-window analysis, and additional modifications were made to the dFNC codes to enable regression analysis.

Detrending, despiking, and low-pass filtering (<0.15 Hz) were applied to the time series of the ICN components. The correlation value was used as the connectivity metric in consecutive time windows. The size of the selected time windows was chosen as 30 TR (60 s), and the shifting amount for consecutive time windows was chosen as 1 TR (2 s). The selection of the time window width was carefully balanced to avoid being excessively wide, which could lead to a loss of dynamism; this also prevents it from being too short, which would increase sensitivity to noise (22). In addition, each window was convolved with a Gaussian kernel with a 3 TR FWHM to eliminate possible discontinuities due to sudden drops at the beginning and end of the time windows. Connectivity calculations were made for a total of 180 windows, resulting in dFNCs comprising 180 values. The $PETCO_2$ signal for which the regression analysis will be performed was averaged within the same time window and subsequently reduced to 180 values.

Statistical Analysis for Regression

The randomize command in FSL was employed for the statistical inference of the regression coefficients using non-parametric permutation (500 permutations) (23). Multiple-comparison (family-wise error) correction was applied for each ICN component pair, with the significance threshold set at $pFWE < 0.05$.

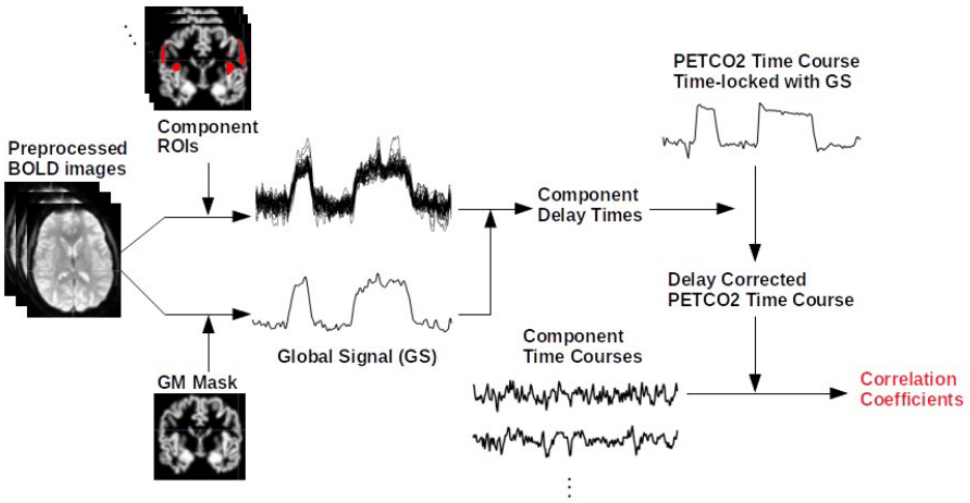

Figure 1. Correlation analysis pipeline with time delay correction for each component time course.

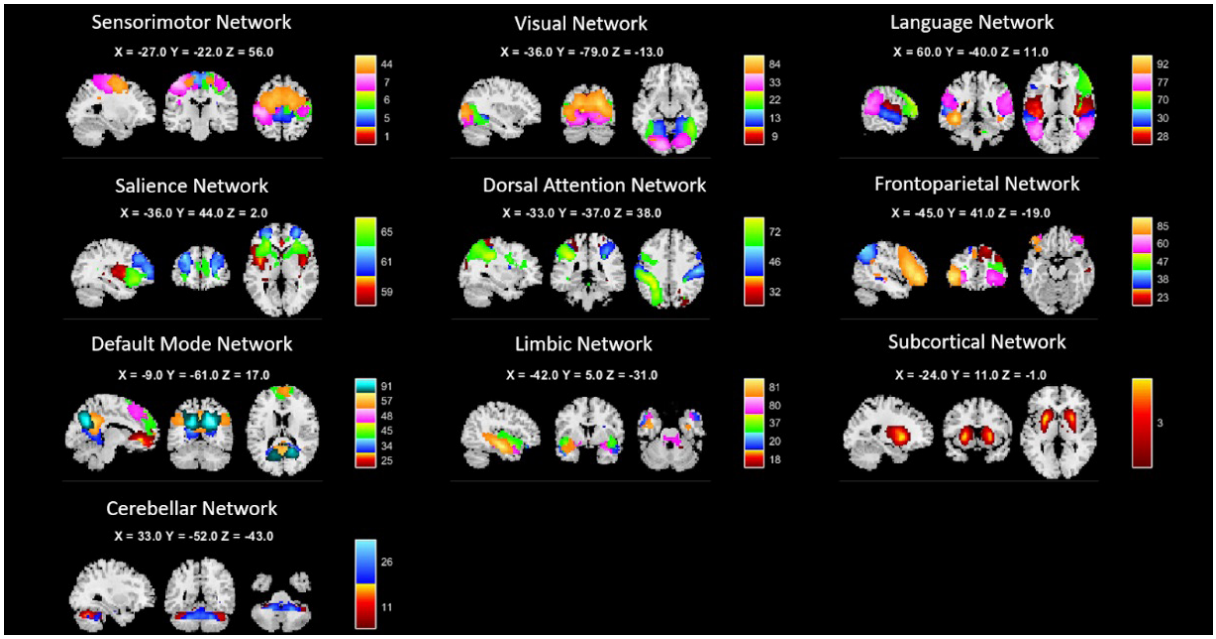

Figure 2. Grouped spatial maps of the ICN components determined to be included in a connectivity network as a result of the GICA analysis.

RESULTS

Group Independent Component Analysis Results

Following the GICA analysis, a total of 100 independent components were acquired. Upon evaluation, 40 of these 100 components were identified as network components within the ICNs (Figure 2).

The default mode network includes six different ICs covering the posterior cingulate cortex, medial prefrontal cortex, and left lateral parietal regions. The frontoparietal network contains five ICs that comprise the left lateral prefrontal cortex and left and right posterior parietal cortices. The dorsal attention network consists of the left inferior parietal sulcus and right

Table 1. ICN components and their significance levels showing significant correlation with the $PETCO_2$ signal change

Comp. Number	Corresponding ICN	mean r-value	p-value
44	Sensorimotor, Superior	0.42	0.001
9	Visual, Medial	0.38	<0.001
32	Dorsal Attention, IPS(L)	0.46	<0.001
46	Dorsal Attention, IPS(R)	0.35	<0.001
23	FrontoParietal, PPC (R)	0.36	<0.001
47	Frontoparietal	0.32	<0.001
25	Default Mode, MPFC	0.34	<0.001
45	Default	0.32	0.001
57	Default Mode, PCC	0.41	<0.001
37	Limbic	0.27	0.001
26	Cerebellar, Anterior	0.29	<0.001

inferior parietal sulcus. The visual network is represented by five ICs that correspond to the right lateral, medial, and occipital ICs. The sensorimotor network consists of five ICs that cover the superior, left, and right lateral sensorimotor regions. The cerebellar network encompasses the anterior cerebellar ICs. The salience network comprises the left insula and the right prefrontal cortex region. The language network is represented by the left and right posterior superior temporal gyri and the right inferior parietal gyrus. Additionally, the limbic network includes five ICs, and the subcortical network consists of one IC.

Correlation Analysis Results Between ICN Components and $PETCO_2$ Signal Change

The subject-wise average temporal shifts applied to the time series of the network components prior to the correlation analysis were in the range of -1.30 to +1.36 seconds with respect to the GS. Significant ICN components exceeding the Bonferroni-corrected significance threshold ($p<0.05/40$) as a result of the two-sample t-test are shown in Table 1. According to the two-sample t-test, the ICN components that show a significant correlation with the $PETCO_2$ signal include: the superior component of the sensorimotor network; the medial component of the visual network; the left and right intraparietal sulcus components of the dorsal attention network; the posterior parietal cortex component of the frontoparietal network; the medial prefrontal cortex and posterior parietal cortex components of the default mode network; the limbic network; and the anterior component of the cerebellar network.

Regression Analysis Results Between dFNC and the $PETCO_2$ Change

The matrix of t-values (Figure 3) resulting from the regression analysis revealed relationships between the dFNC values and $PETCO_2$ time course. Notably, significant cells were observed within the three components of the visual network (visual, lateral (R), visual, occipital, visual, medial), despite the absence of significant correlations between their time courses and the $PETCO_2$ signal. Additionally, other significant findings include dynamic connectivity between the sensorimotor, lateral (R) component and the subcortical network, as well as between the sensorimotor, lateral (R) component and language, posterior part of the superior temporal gyrus (pSTG)(L) component. These results highlight specific interactions influenced by the $PETCO_2$ signal within the examined ICNs.

DISCUSSION

This study has used fMRI data, which captures cognitive brain activity, while measuring cerebrovascular reactivity through hypercapnic stimulation. During fMRI, hypercapnic stimulation increases the blood flow rate due to vasodilation, thus increasing the measured functional response. GICA was performed to detect intrinsic connectivity networks in this dataset. Thus, the study has investigated how non-neuronal hypercapnic stimulation affects ICNs that have been obtained using fMRI data. The components obtained as a result of the GICA were examined, and the components representing ICNs were successfully identified. In this respect, the ICNs defined in the literature have been shown to be detectable under conditions definable as the stress testing of brain vessels. Recent studies are found in the literature that support this finding. Hou et al. (24) measured resting state and CVR in two separate fMRI scans and reported static functional connectivity metrics to be calculable despite the presence of hypercapnic stimulation. However, dynamic connectivity analyses were not performed on the time series of the network components obtained with GICA, and they did not investigate their correlation with the $PETCO_2$ signal.

Lewis et al. (25) investigated static and dynamic connectivity in CVR data and interpreted the correlation between the detected ICNs and the $PETCO_2$ signal in the study as the CVR of these networks. They reported the sensorimotor and visual networks to exhibit high CVR. These findings are consistent with the current study's finding that the dynamic connectivity of the sensorimotor and visual networks is modulated by the $PETCO_2$ signal.

In addition, the high correlation between ICN and $PETCO_2$ time series has been suggested as being attributable to the spare capacity the cerebral circulation has for increasing CBF (i.e., the vascular reserve of the relevant network) (25). Meanwhile, Tong et al. (26) reported GICA to be able to produce networks that do not actually exist by applying synthetic time delays to the BOLD signal. They interpreted this as the ICA being highly sensitive

Experimed 2024; 14(1): 54-60

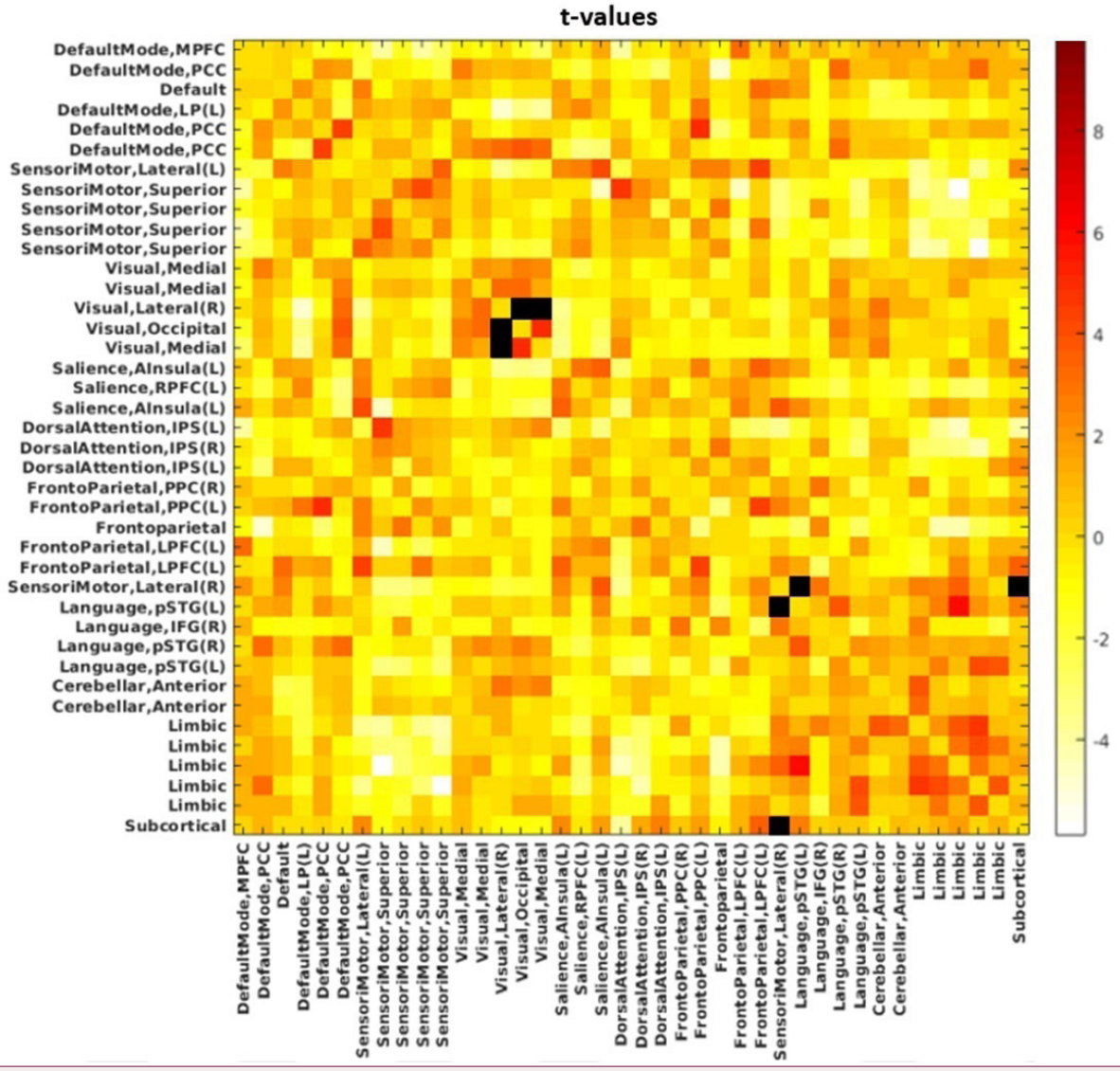

Figure 3. Matrix of t-values resulting from the regression analysis between the dFNC values and $PETCO_2$ time course. Each cell represents the statistical significance of the relationship between the corresponding pair of dFNC values and $PETCO_2$, providing insights into the modulatory effect of $PETCO_2$ on dynamic functional connectivity within ICNs. The color bar represents t-values, with statistically significant pairs being shown in black.
(MPFC = Medial Prefrontal Cortex; PCC = Posterior Cingulate Cortex; LP = Lateral Parietal; RPFC = Rostral Prefrontal Cortex; AInsula = Anterior Insula; IPS = Inferior Parietal Sulcus; LPFC = Lateral Prefrontal Cortex, IFG = Inferior Frontal Gyrus, pSTG = Posterior Superior Temporal Gyrus)

to time delays in the BOLD signal. When evaluated from this perspective, the correlation between the $PETCO_2$ time series and ICN time series may be due to network-specific delays in the systemic signal. In this case, the observed correlation may be an indicator of the systemic oscillations reflected onto the network.

The current study's findings show the network components to be similar to the $PETCO_2$ time series, whereas network components that do not show a direct correlation may have significant modulation with $PETCO_2$ in a dynamic connectivity analysis. The facts that hypercapnic stimulation affected the connectivity metrics in nine of the 10 networks and that this finding indicates a more widespread effect than shown in the literature can be interpreted in two ways. The first reason may be that, when determining ICNs, they are separated into many components, resulting in components with a high contamination. The second reason may be that, through this study's unique approach, a second time delay correction made for each network component has allowed the effect to be revealed more precisely.

Despite the use of non-parametric statistics, the study is limited by a small sample size. Because the dataset originated from a different study, a larger sample could not be obtained, nor could a power analysis be conducted. As a result, care should be used when generalizing the findings, as the small sample size may limit statistical power and increase the possibility of bias.

CONCLUSION

The CVR to a hypercapnic stimulus exerts a significant influence on the alterations observed in the BOLD fMRI signal. This non-neuronal effect manifests notably in ICN components derived through the GICA technique. The intricate relationship between CVR and the BOLD fMRI signal underscores the importance of acknowledging non-neuronal factors in the study of neural networks. As scientists investigate the functional connectivity of the brain, especially by employing methodologies such as GICA, incorporating non-neuronal influences becomes critical for precise interpretations and robust network connectivity metrics.

Ethic Committee Approval: The data used in the study was downloaded from Oxford University Research Archive. Ethics committee approval is not required.

Peer-review: Externally peer-reviewed.

Author Contributions: Conception/Design of Study- A.B., I.I.; Data Analysis/Interpretation- I.I.; Drafting Manuscript- A.B.; Critical Revision of Manuscript- A.B.; Final Approval and Accountability- A.B.

Conflict of Interest: The authors declare that they have no competing interests.

Financial Disclosure: This study was funded by the Scientific and Technological Research Council of Turkey (TUBITAK) ARDEB 3501 Grant No: 122S188.

REFERENCES

1. Friston KJ. Functional and effective connectivity in neuroimaging: A synthesis. Hum Brain Mapp 1994; 2(1–2): 56–78.
2. Biswal BB, Yetkin F, Haughton VM, Hyde JS. Functional connectivity in the motor cortex of resting human brain using echo-planar MRI. Magn Reson Med 1995; 34(4): 537-41.
3. Fox MD, Raichle ME. Spontaneous fluctuations in brain activity observed with functional magnetic resonance imaging. Nat Rev Neurosci 2007; 8(9): 700–11.
4. Raichle ME, MacLeod AM, Snyder AZ, Powers WJ, Gusnard DA, Shulman GL. A default mode of brain function. Proc Natl Acad Sci U S A. 2001; 98(2): 676–82.
5. Calhoun VD, Adali T, Stevens MC, Kiehl KA, Pekar JJ. Semi-blind ICA of fMRI: A method for utilizing hypothesis-derived time courses in a spatial ICA analysis. Neuroimage 2005; 25(2): 527–38.
6. Beckmann CF, Smith SM. Probabilistic independent component analysis for functional magnetic resonance imaging. IEEE Trans Med Imaging 2004; 23(2): 137-52.
7. Sleight E, Stringer MS, Marshall I, Wardlaw JM, Thrippleton MJ. Cerebrovascular Reactivity Measurement Using Magnetic Resonance Imaging: A Systematic Review. Front Physiol 2021; 12: 643468.
8. Liu TT. Reprint of "Noise contributions to the fMRI signal: An Overview". Neuroimage 2017; 154: 4–14.
9. Blockley NP, Harkin JW, Bulte DP. Rapid cerebrovascular reactivity mapping: Enabling vascular reactivity information to be routinely acquired. Neuroimage 2017; 159: 214–23.
10. Sobczyk O, Battisti-Charbonney A, Poublanc J, Crawley AP, Sam K, Fierstra J, et al. Assessing cerebrovascular reactivity abnormality by comparison to a reference atlas. J Cereb Blood Flow Metab 2015; 35(2): 213–20.
11. Jenkinson M, Bannister P, Brady M, Smith S. Improved optimization for the robust and accurate linear registration and motion correction of brain images. Neuroimage 2002; 17(2): 825–41.
12. Jenkinson M, Beckmann CF, Behrens TE, Woolrich MW, Smith SM. FSL. Neuroimage 2012; 62(2): 782–90.
13. Greve DN, Fischl B. Accurate and robust brain image alignment using boundary-based registration. Neuroimage 2009; 48(1): 63–72.
14. Smith SM, Brady JM. SUSAN-A new approach to low level image processing. Int J Comput Vis 1997; 23(1): 45–78.
15. Calhoun VD, Adali T. Multisubject independent component analysis of fMRI: a decade of intrinsic networks, default mode, and neurodiagnostic discovery. IEEE Rev Biomed Eng 2012; 5: 60–73.
16. Du Y, Fan Y. Group information guided ICA for fMRI data analysis. Neuroimage 2013; 69: 157–97.
17. Griffanti L, Douaud G, Bijsterbosch J, Evangelisti S, Alfaro-Almagro F, Glasser MF, et al. Hand classification of fMRI ICA noise components. Neuroimage 2017; 154: 188–205.
18. Nieto-Castanon A. Handbook of functional connectivity magnetic resonance imaging methods in CONN. Boston, MA: Hilbert Press; 2020.
19. Yeo BT, Krienen FM, Sepulcre J, Sabuncu MR, Lashkari D, Hollinshead M, et al. The organization of the human cerebral cortex estimated by intrinsic functional connectivity. J Neurophysiol 2011; 106(3): 1125–65.
20. Frederick B. Rapidtide, ver. 2.2.7 [computer program]. Belmont (MA): GitHub; 2022. [cited 20 January 2024]. Available from: https://github.com/bbfrederick/rapidtide.
21. Allen EA, Erhardt EB, Wei Y, Eichele T, Calhoun VD. Capturing inter-subject variability with group independent component analysis of fMRI data: A simulation study. Neuroimage 2012; 59(4): 4141–59.
22. Vergara VM, Mayer AR, Kiehl KA, Calhoun VD. Dynamic functional network connectivity discriminates mild traumatic brain injury through machine learning. Neuroimage Clin 2018; 19: 30–7.
23. Winkler AM, Ridgway GR, Webster MA, Smith SM, Nichols TE. Permutation inference for the general linear model. Neuroimage 2014; 92: 381–97.
24. Hou X, Liu P, Gu H, Chan MY, Li Y, Peng S, et al. Estimation of brain functional connectivity from hypercapnia BOLD MRI data: Validation in a lifespan cohort of 170 subjects. Neuroimage 2019; 186: 455–63.
25. Lewis N, Lu H, Liu P, Hou X, Damaraju E, Iraji A, et al. Static and dynamic functional connectivity analysis of cerebrovascular reactivity: An fMRI study. Brain Behav 2020; 10(6): e01516.
26. Tong Y, Hocke LM, Fan X, Janes AC, Frederick Bd. Can apparent resting state connectivity arise from systemic fluctuations? Front Hum Neurosci 2015; 9: 285.